Nonlinear dust acoustic waves and shocks

R. L. Merlino, J. R. Heinrich, S.-H. Hyun, and J. K. Meyer

Citation: Phys. Plasmas **19**, 057301 (2012); doi: 10.1063/1.3693972
View online: http://dx.doi.org/10.1063/1.3693972
View Table of Contents: http://pop.aip.org/resource/1/PHPAEN/v19/i5
Published by the American Institute of Physics.

Nonlinear dust acoustic waves and shocks[a)]

R. L. Merlino,[b)] J. R. Heinrich, S.-H. Hyun, and J. K. Meyer
Department of Physics and Astronomy, The University of Iowa, Iowa City, Iowa 52242, USA

(Received 16 December 2011; accepted 23 December 2011; published online 19 March 2012)

We describe experiments on (1) nonlinear dust acoustic waves and (2) dust acoustic shocks performed in a direct current (DC) glow discharge dusty plasma. First, we describe experiments showing nonlinear dust acoustic waves characterized by waveforms of the dust density that are typically sharper in the wave crests and flatter in the wave troughs (compared to sinusoidal waves), indicating the development of wave harmonics. We discuss this behavior in terms of a second-order fluid theory for dust acoustic waves. Second, experimental observations of the propagation and steepening of large-amplitude dust acoustic waves into dust acoustic shock waves are presented. The observed shock wave evolution is compared with numerical calculations based on the Riemann solution of the fully nonlinear fluid equations for dust acoustic waves. © *2012 American Institute of Physics*. [http://dx.doi.org/10.1063/1.3693972]

I. INTRODUCTION

Dust acoustic waves are propagating dust density fluctuations, analogous to ion sound waves in an electron/ion plasma, with the role of the positive ions replaced by heavy, charged dust particles.[1] Because the charge to mass ratio of the dust particles is relatively low, <1, the phase velocity of the dust acoustic waves is well below the ion thermal speed in a typical laboratory discharge plasma. Typical wavelengths and frequencies for the dust acoustic wave are $\lambda < 1$ cm, and $f \sim$ few to tens of Hz. A unique feature of dust acoustic waves is that the micron size particles can be imaged using light scattering and video cameras, which allows experimenters to follow the collective motion of the dust particles in the wave.

The dust acoustic wave was discovered theoretically in 1989 (Ref. 2) and reported by Rao, Shukla, and Yu (RSY).[3] RSY derived the dispersion relation for small amplitude dust acoustic waves and also obtained a Boussinesque-type equation for weakly nonlinear waves. They also foresaw that the dust charge would not be fixed, but would be affected by the presence of the fluctuating potentials in the plasma, a unique and defining characteristic of dusty plasmas as compared to multi-ion component plasmas. The linear dispersion relation for dust acoustic waves was also contained in the general dispersion relation derived by D'Angelo[4] for low-frequency electrostatic waves in a homogeneous, magnetized dusty plasma.

Chu, Du, and I reported[5] observations of large amplitude, low frequency oscillations in a dusty plasma formed by the generation of SiO_2 dust particles in silane/oxygen/argon radio frequency (rf) discharge. The fluctuations had a typical frequency of 12 Hz and a wavelength of 0.5 cm. These observations were interpreted by D'Angelo[6] as very likely being dust acoustic waves. Barkan *et al.*[7] observed self-excited dust acoustic waves with a wavelength of 0.6 cm propagating at a speed of $\sim$ 9 cm/s in a dusty plasma suspended in an anode glow discharge formed in a Q machine plasma. They obtained a single frame video image of the dust acoustic wave pattern showing enhanced light scattering from the wave crests. The waves were of very large amplitude, often with $\Delta n_d / n_d \sim 1$. A measurement of the dust acoustic wave dispersion relation (in the long wavelength regime) was performed by Thompson *et al.*[8] in a dc glow discharge dusty plasma. Although the waves were self-excited, a sinusoidal voltage modulation was applied to the anode (in addition to the dc bias) at frequencies in the range of 5–40 Hz. For sufficiently large voltage modulations, the dust acoustic waves could be driven at the frequency of the applied modulation. For each applied frequency, the wavelength was measured directly from the single frame dust acoustic wave images and the dispersion relation was obtained. Subsequently, further work on understanding the synchronization of dust density waves in anodic plasmas has been performed.[9–12]

One ubiquitous feature of self-excited dust acoustic waves alluded to above is that the waves are typically of high amplitude. In addition to the experiments cited above,[5,7–12] large amplitude self-excited dust acoustic waves have been reported by Prabhakara and Tanna,[13] Fortov *et al.*,[14] Thomas and Merlino,[15] Schwabe *et al.*,[16] and Teng *et al.*[17] Although the cited experiments differed in that some were dc driven while other were rf-driven, they all had one distinctive element—the presence of an ion current, typically associated with an ion streaming velocity on the order of the ion thermal speed. The relative streaming of the ions through the dust fluid produces the instability which excites the dust density (acoustic) waves.[18] This can be demonstrated using either fluid theory[18] or kinetic theory.[19] It appears that under typical operating conditions (discharge current and neutral pressures) of both the dc and rf-driven dusty plasmas, the ion drift speed is not just above the critical value for wave excitation, but well-above critical, so that large-amplitude dust acoustic waves are excited.

There have been some observations of the linear growth phase of dust (density) acoustic waves. Trottenberg *et al.*[9] measured the spatial growth rate of self-excited dust acoustic

[a)]Paper BI2 5, Bull. Am. Phys. Soc. **56**, 24 (2011).
[b)]Invited speaker. Electronic mail: robert-merlino@uiowa.edu.

waves observed in a weakly magnetized anodic discharge plasma by applying the singular value decomposition technique. The wave amplitude appeared to grow exponentially up to values of $n_d/n_{d0} \sim 0.3$. Flannigan and Goree[20] observed the spatial growth of self-excited dust density waves in a capacitively coupled parallel-plate rf discharge. A glass box was placed on the lower (powered) electrode, which trapped dust particles in many horizontal layers. Dust density waves were observed to propagate downward, toward the lower electrode, in the direction of the ion drift. The experiment was started at a relatively high neutral pressure (426 mTorr), where the dust density waves were not observed due to dust-neutral damping. When the neutral pressure was decreased to 424 mTorr, the dust density waves appeared, and the wave amplitude was measured as the waves propagated downward. Exponential growth of the waves was observed, indicating a period of linear wave growth. The wave amplitude eventually saturated, indicating that onset on nonlinearities.[21] Heinrich *et al.*[22] observed linear dust acoustic waves in a quiescent drifting dusty plasma and measured the temporal growth rate. This experiment was performed in a weakly magnetized anodic discharge plasma but with the addition of a secondary dust cloud that was initially trapped in the potential well formed by a mesh electrode placed roughly 15 cm downstream of the anode. Although dust acoustic waves were present in the primary anode discharge dusty plasma, the secondary cloud was completely free of dust acoustic waves. When the bias on the mesh was suddenly switched off (to floating), the secondary cloud began to drift toward the primary cloud. When the secondary cloud was ~7 cm from the primary cloud, dust acoustic waves began appearing in the secondary cloud. The dust acoustic waves grew exponentially through the linear growth phase, with the wave amplitude eventually saturating and the waves exhibiting nonlinear characteristics. The dust acoustic waves that were observed during the early phases of growth were sinusoidal in form.

This paper will concentrate on weakly nonlinear dust acoustic waves and highly nonlinear dust acoustic shock waves. We attempt to interpret the nonlinear development of the waves in terms of the simplest possible fluid description of dust acoustic waves.[23] For the weakly nonlinear waves, we will show that the nonlinearity can be understood in terms of the appearance of a first harmonic wave in addition to the fundamental mode. A characteristic feature of the observed waves is that the wave crests are sharper and the wave troughs are flatter compared to purely sinusoidal waves. This is similar to deep ocean water waves, where the application of Stokes' theory has been successful in modeling the waveforms.[24] The continuity and momentum equation for the dust acoustic waves will be expanded to second order, and the appearance of the second harmonic wave follows naturally. The dust acoustic shock waves[25] cannot be treated as a weakly nonlinear system. In this case, the fully nonlinear fluid equations must be solved numerically, following the theory of Eliasson and Shukla.[26]

In Sec. II, we briefly summarize the basic equations and assumptions of the fluid theory of dust acoustic waves that will be developed further and applied to nonlinear waves and shocks. The experimental set-up and methods will be described in Sec. III. Section IV presents the results of the weakly nonlinear dust acoustic waves, and Sec. V presents the dust acoustic shock wave results and comparison with numerical calculations. Section VI contains a brief summary and conclusions.

II. FLUID DESCRIPTION OF NONLINEAR DUST ACOUSTIC WAVES

Our goal in this article is to provide an analysis of nonlinear dust acoustic waves and shocks that captures the essential physics of the structures. Keeping this in mind, we proceed with the simplest fluid description with the following assumptions: (i) the dust will be treated as a cold fluid, $T_d = 0$; (ii) the dust charge is constant; (iii) the charge neutrality condition will be assumed; (iv) there are no dissipation mechanisms present; (v) the waves are planar (1-D). Under these conditions, the system is described by the (nonlinear) continuity and momentum equations

$$\frac{\partial n_d}{\partial t} + u_d \frac{\partial n_d}{\partial x} + n_d \frac{\partial u_d}{\partial x} = 0, \tag{1a}$$

$$\frac{\partial u_d}{\partial t} + u_d \frac{\partial u_d}{\partial x} - \frac{eZ_d}{m_d} \frac{\partial \varphi}{\partial x} = 0, \tag{1b}$$

where n_d is the dust density, u_d is the dust fluid velocity, $eZ_d = Q_d$ is the dust charge (taken to be negative), m_d is the dust mass, and φ is the electric potential. Since the phase speed of the dust acoustic wave is well below both the electron and ion thermal speeds, the electrons and ions are taken to be in Boltzmann equilibrium,

$$n_e = n_{e0} \exp(e\varphi / kT_e), \tag{2a}$$

$$n_i = n_{i0} \exp(-e\varphi / kT_i), \tag{2b}$$

where $n_{e(i)}$ is the electron (ion) density and $T_{e(i)}$ is the electron (ion) temperature. The model is completed by taking $\partial^2 \varphi / \partial x^2 = 0$, which amounts to the neglect of dispersive effects and implies the neutrality condition

$$n_i = n_e + Z_d n_d. \tag{3}$$

III. EXPERIMENTAL SET-UP AND METHODS

The experiments were performed in a direct current (DC) glow discharge device shown schematically in Fig. 1. A 3.2 cm diameter disk electrode (insulated on its back side) was located on the axis and near the center of a large, electrically grounded chamber, approximately 90 cm in length by 60 cm in diameter. The disk served as the anode with the chamber as the cathode of a dc glow discharge in argon operated at a pressure of 100–150 mTorr. Typical discharge voltage and current were $(V_d, I_d) = (300\ V, 5\ mA)$. A uniform longitudinal magnetic field of 3–10 mT was applied to provide weak confinement of the electrons which resulted in the formation of an elongated anode glow ("firerod"[27]) that extended ~10–20 cm from the anode. A double Langmuir

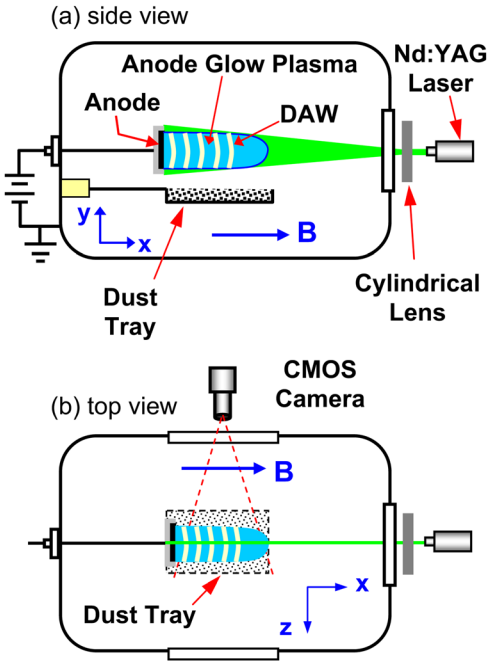

FIG. 1. (Color online) Schematic diagram of the dc glow discharge dusty plasma device, (a) side view, and (b) top view. The anode glow plasma is formed on a 3.2 cm diameter anode disk and is weakly confined as an elongated "firerod" by a longitudinal magnetic field. Dust is incorporated into the plasma from a floating tray located below the anode. The dust behavior is observed using laser light scattering and fast video cameras.

probe was used[28] to measure the ion density (n_i) and electron temperature (T_e) in the firerod, yielding $n_i \sim 10^{14}$ m^{-3} and $T_e \approx 2.5$ eV. The ion temperature in glow discharges is approximately the same as the neutral temperature. An emissive probe was used to measure the potential distribution along the axis of the anode and to determine the axial electric field which was $E \approx 200$ V/m.

Dust particles were introduced into the glow discharge from a floating tray located below the anode. The dust was a fine kaolin powder with sizes in the range of a few microns. When the discharge is initiated, some dust from the tray is lifted up and incorporated into the discharge over a time span of a few minutes. Once a substantial suspension becomes trapped in the plasma, it remains trapped, although there is a decrease in the dust density over a timescale of tens of minutes. The charge on the dust was not measured, but estimates of the charge using the orbital motion limited theory[29] indicate that dust of diameter 1 μm, $Q_d \sim -2000$ elementary charges, i.e., $Z_d \approx 2000$. By analysis of the video images of the dust, we estimate that the dust density $n_d \approx 1 \times 10^{10}$ m^{-3}. The dust suspension is imaged using a vertical sheet (1 mm thickness) of 532 nm laser light and either a CCD camera operating at a frame rate of 30 fps, or a CMOS video camera[30] capable of frame rates exceeding 1000 fps. The dust density is a linear function of the scattered light intensity. The laser sheet can be moved horizontally to image various vertical slices of the dust suspension.

Propagating dust acoustic waves spontaneously appeared in the dust suspension once a sufficient dust density had accumulated. The dust acoustic waves propagated in the direction of the ion drift, away from the anode and had the

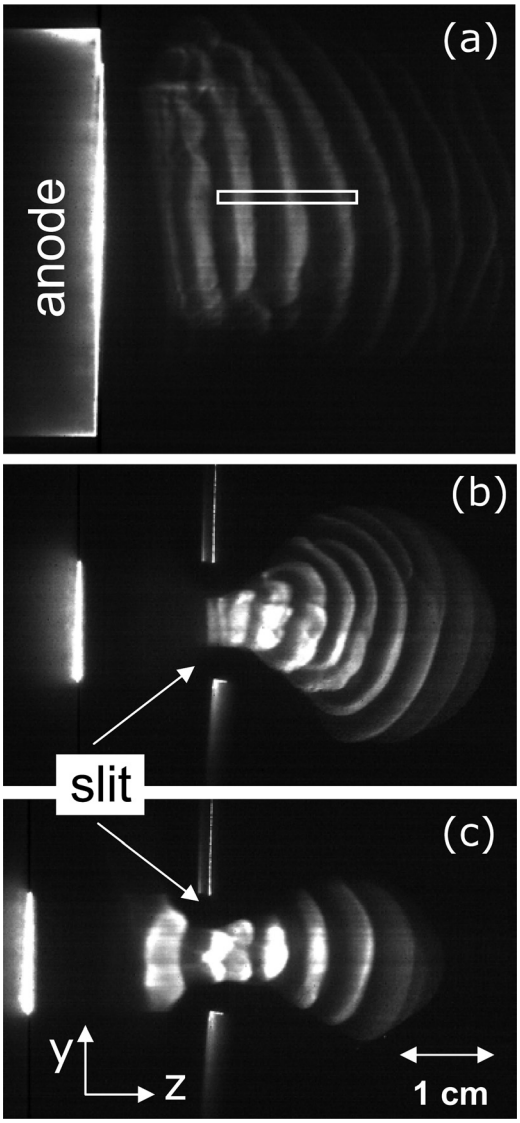

FIG. 2. Single frame video images of (a) quasi-planar dust acoustic waves, and cylindrical dust acoustic waves and shocks produced by inserting a floating slit in front of the anode, (b) and (c). The structure of the dust suspension depends on the location of the slit relative to the anode. Dust acoustic shock waves were observed when the slit was farthest from the anode, as in (c).

appearance of bright vertical bands of enhanced scattered light intensity (wave compressions) separated by regions of much lower scattered light intensity (wave rarefactions). A single frame video image of a typical dust acoustic wave pattern is shown in Fig. 2(a). The wavelength can be measured directly from these images, and the wave phase speed determined by following the spatial progression of a particular wavefront. The nonlinearity of the dust acoustic wave shown in Fig. 2(a) will be demonstrated in Sec. IV.

For some experiments, a 1 cm wide slit was placed in front of the anode, at a variable distance from it. Since the slit floated at a negative potential, the negatively charged particles were repelled by it, and the boundary of the dust cloud conforms to the contours of electrical potential near the slit. The shape of the cloud boundary and the location at which the dust acoustic waves begin being excited could be controlled by changing the position of the anode relative to the slit. Two possible anode/slit configurations are shown in

Figs. 2(b) and 2(c). Using the configuration of Fig. 2(b), cylindrical dust acoustic waves were produced. For the configuration in Fig. 2(c), the dust acoustic waves are first excited on the anode side of the slit. In this configuration, the waves propagate through a type of electrostatic nozzle and give rise to strongly nonlinear dust acoustic waves which evolve into dust acoustic shocks, which will be described in Sec. V.

Further details of the experimental configurations and imaging techniques can be found in Refs. 22 and 25.

IV. NONLINEAR DUST ACOUSTIC WAVES

A. Experimental results

A feature of weakly nonlinear waves is their non-sinusoidal waveform, in particular waveforms that exhibit sharper wave crests and flatter wave troughs. The dust acoustic waveform shown in Fig. 2(a) has these characteristics. The waveform of the scattered light intensity (~dust density) in the region of interest (ROI) designated by the rectangular box in Fig. 2(a) is shown as the circles plotted in Fig. 3(a). The solid line in this figure is the light intensity $\langle I \rangle$, averaged over a long time series of the dust acoustic wave. The wave amplitudes in the wave crests, $\Delta n_d/\langle n_d \rangle$, where $\Delta n_d = n_d - \langle n_d \rangle$, for the wave crests at x = 2 mm, 6.5 mm, and 11 mm are 0.66, 0.85, and ~1, respectively, showing clearly the nonlinear nature of the waves. Note that the wave troughs have somewhat smaller amplitudes and are considerably flatter than the peaked crests. For this case shown, which is rather typical of the dust acoustic waves that we have recorded, the dust density does not go to zero in the wave troughs. To analyze the nonlinearity of this wave, it is convenient to plot Δn_d rather than n_d, and this is shown as the plotted circles in Fig. 3(b). In this representation, which is one that is commonly used in acoustics,[31] the perturbations in the dust density are plotted on a scale with the baseline corresponding to the ambient density.

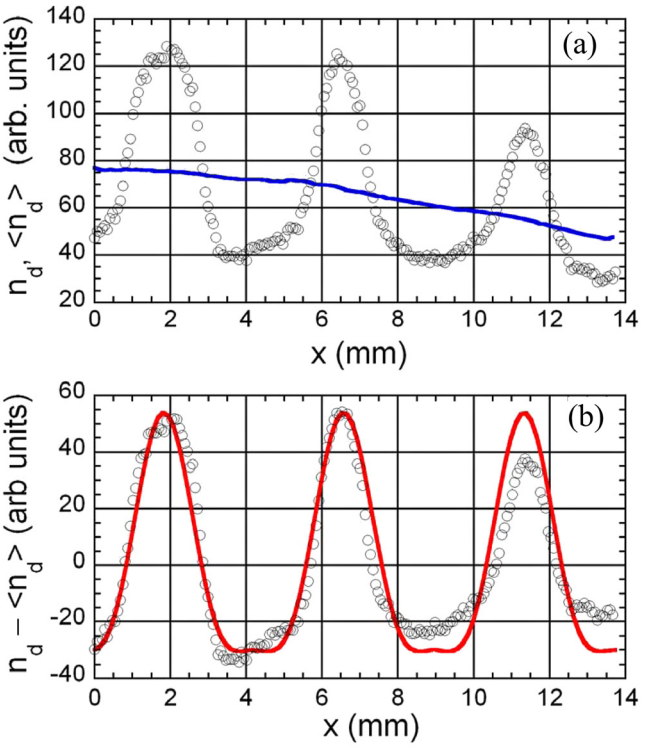

FIG. 3. (Color online) Dust density profiles obtained from single-frame video images of scattered light intensity. (a) Circles: a typical nonlinear dust acoustic waveform. Solid line: average dust density obtained by averaging the scattered light intensity over a video record containing thousands of wave periods. (b) Solid line: dust acoustic waveform fit using Eq. (5).

B. Second-order dust acoustic wave theory

We will interpret the non-sinusoidal dust acoustic waveform of the type shown in Fig. 3(a) by developing a second-order wave theory using Eqs. (1) through (3), which we briefly summarize here.[32] If ψ represents any of the variables (n_e, n_i, n_d, u_d, φ), it is expanded in a perturbation series with small parameter ε as $\psi = \psi_0 + \varepsilon\psi_1 + \varepsilon^2\psi_2$, with $u_{d0} = 0$, and $\varphi_0 = 0$. The Boltzmann relations (Eq. (2)) are expanded to second order in φ and combined with the charge neutrality condition, so that the first and second-order wave potentials can be expressed in terms of the first and second-order dust densities. When the expansion of the continuity and momentum equations is carried out to second order, the following second-order dust acoustic wave equation is obtained for n_{d2}

$$\frac{\partial^2 n_{d2}}{\partial x^2} - \frac{1}{C_{DA}^2}\frac{\partial^2 n_{d2}}{\partial t^2} = A\frac{\partial^2 n_{d1}^2}{\partial x^2} + B\frac{\partial^2 n_{d1}^2}{\partial x \partial t}, \tag{4}$$

where $C_{DA} = \omega_{pd}\lambda_D$, $\omega_{pd} = (e^2 Z_d^2 n_{d0}/\varepsilon_o m_d)^{1/2}$, $A = A_2/A_1$ $-\omega^2/(2k^2 n_{d0} C_{DA}^2)$, $B = \omega/(k n_{d0} C_{DA}^2)$ $A_1 = eZ_d\lambda_D^2/\varepsilon_o$, A_2 $= e^3(Z_d)^2\lambda_D^6(1-\alpha\tau^2)/\left(2\varepsilon_o^2 kT_i\lambda_{Di}^2\right)$, $\alpha = n_{e0}/n_{i0}$, and $\tau = T_i/T_e$, $\lambda_D = \lambda_{De}\lambda_{Di}/\sqrt{\lambda_{De}^2 + \lambda_{Di}^2}$, and $\lambda_{Ds} = (\varepsilon_o kT_s/e^2 n_{s0})^{1/2}$.

Equation (4) is the second-order equation for dust acoustic waves and is very similar in form to the second-order equation for sound waves,[33] in which the first order terms on the right hand side appear as *source terms* for the second-order wave equation. Since the source terms are products of first order terms, which can be regarded as known, these terms allow for the calculation of the second-order contribution to the dust acoustic waves. For plane wave solutions for $n_{d1} \sim \exp[i(kx - \omega t)]$, the source terms in Eq. (4) give rise to the second harmonic $\exp[2i(kx - \omega t)]$. It is clear that carrying out the perturbation analysis to second order leads not only to quantitative corrections to the first order quantities but also to add qualitatively new effects that are not contained in a linear wave analysis.[34] Dropping the expansion parameter ε, the dust density to second order can now be written as $n_d = n_{d0} + n_{d1} + n_{d2}$ or the excess dust density as $\Delta n_d \equiv n_d - n_{d0} = n_{d1} + n_{d2}$. Since the second-order term involves the second harmonic, the wave solution can then be written to second order at an arbitrary time t = 0 as

$$\Delta n_d(x,0) = \tilde{n}_{d1}\cos(kx - \omega t + \vartheta) + \tilde{n}_{d2}\cos[2(kx - \omega t + \vartheta)], \tag{5}$$

where $\tilde{n}_{d1}$ and $\tilde{n}_{d2}$ are the first- and second-order amplitudes and ϑ is an arbitrary phase factor. We have performed a fit of Eq. (5) to the experimental dust acoustic waveform shown in

Fig. 3 which is shown as the solid line in Fig. 3(b). The wavelength was measured as the distance between successive crests and was $\lambda = 4.7$ mm. The amplitudes $\tilde{n}_{d1}$ and $\tilde{n}_{d2}$ were then chosen to give the best fit which was determined to be

$$\Delta n_d(x,0) = 42[\cos\{(2\pi/4.7)x - 8.7\} + 0.29\cos\{2[(2\pi/4.7)x - 8.7]\}],$$

so that the nonlinear content of the wave, in this case, was ~30%. The addition of the second harmonic term gives a reasonable representation of the observed dust acoustic wave and captures the sharper crests and flatter troughs.

V. DUST ACOUSTIC SHOCKS

A. Experimental results

Section IV dealt with weakly nonlinear dust acoustic waves in which the nonlinear waveforms could be represented by including one higher harmonic component. If the wave amplitude increases further, additional higher harmonic waves are generated. The effect of the higher harmonics is to change the excess density profiles into a curve with a slowly rising trailing part and a sharply falling front, approaching a saw-tooth character.[35] Carrying out a perturbation-type analysis, of the type done in Sec. IV, to higher orders to attempt to describe the evolution of a highly nonlinear dust acoustic wave into a dust acoustic shock wave becomes intractable, in which case it is more prudent to apply other methods of solving the fully nonlinear continuity and momentum equations, as we will present below. First, the experimental observations of the dust acoustic shock waves will be summarized.

The observations were performed in the device shown in Fig. 1 with the addition of the slit located roughly 1.5 cm in front of the anode, as shown in Fig. 2(c). In this configuration, the dust acoustic waves were first excited on the anode side of the slit and experienced a vertical compression as they pass through the slit. The boundary of the dust suspension is due to the electrostatic structure formed by the floating slit, which resembles a nozzle. As the waves emerged from the slit, they steepened and develop into a series of cylindrical shocks. The evolution of one wave starting at a point just to the right of the slit (designated as t = 0) is shown at successive times in Fig. 4(a). We see that as it propagated the trailing part of the curve is stretched out, while the leading edge is steepened, resulting in a classic saw-tooth-like shock wave. A plot of the position, amplitude, and shock front thickness vs. time is shown in Fig. 5. The shock speed was $V_S \approx 50$ mm/s, which is slightly below but on the order of the dust acoustic speed for our dusty plasma conditions.[25] The decrease in the amplitude was somewhat more rapid than what would be expected alone from a cylindrically spreading wave. The thickness of the shock front, δ, first decreased, then approached a minimum value ~0.3 mm, suggesting that a stationary shock was formed. The observation of a stationary shock implies the presence of a dissipation mechanism(s) which balances the tendency of nonlinear steepening of the shock. Several mechanisms have been proposed for the dissipation that gives rise to stationary shocks. Mamun and Cairns considered strong correlation effects between the dust particles as a potential mechanism,[36] while Gupta *et al.*[37] and Asgari *et al.*[38] investigated the

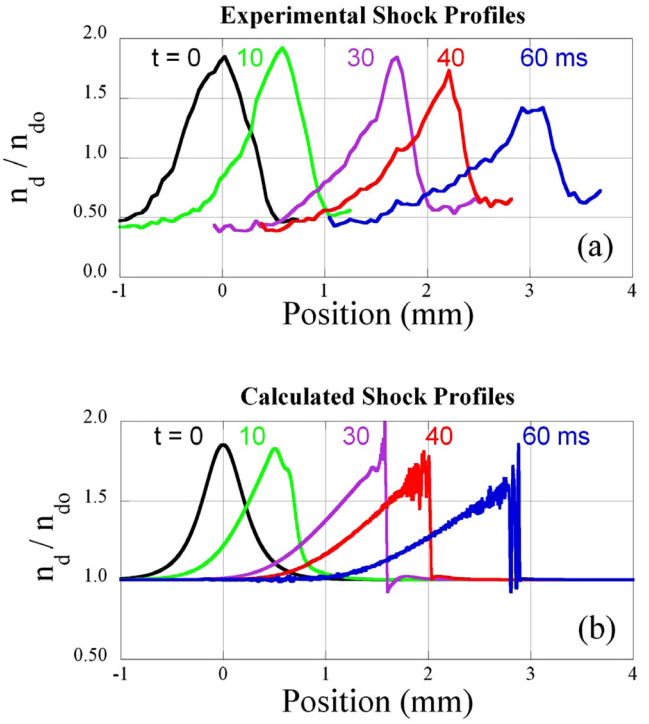

FIG. 4. (Color online) (a) Experimental profiles of the self-steepening of dust acoustic waves into dust acoustic shocks, over 60 ms. The shocks front steepens but reaches a point at which the shock thickness stabilizes to a minimum value. (b) Calculated dust acoustic shock profiles obtained from numerical computations of Eq. (7) using the theory of Ref. 26. The model equations contain no dissipation mechanisms; hence, the numerical results produce non-stationary solutions.

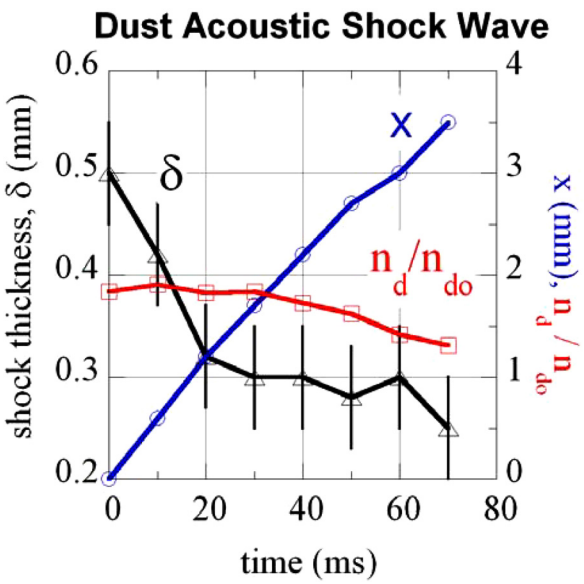

FIG. 5. (Color online) Shock position (x), amplitude (n_d/n_{d0}), and thickness (δ) vs. time obtained from the profiles shown in Fig. 4(a). The shock width stabilizes to a minimum value of roughly 0.3 mm, which is very close to the interparticle spacing.

nonadiabatic charge variation as a possible dissipation mechanism. On the other hand, we find that dust-neutral collisions may be sufficient to explain the limiting shock width. We estimate a dust-neutral mean-free-path $\lambda_{dn} \sim 0.5$–1 mm.[25] The measured shock width is also on the order of the interparticle spacing, $\Delta \approx (3/4\pi n_{d0})^{1/3} \sim 0.3$ mm for $n_{d0} \sim 10^{11}$ m^{-3}, which suggests that the shock width may ultimately be limited by this fundamental length scale.

B. Numerical solutions to the nonlinear fluid equations

The evolution of large-amplitude dust acoustic waves of the type shown in Fig. 4 into dust acoustic shock waves was compared with numerical solutions to the nonlinear dust continuity and momentum equations (Eqs. (1)–(3)) using the theory developed by Eliasson and Shukla.[26] Eliasson and Shukla obtained the Riemann solution[39] for simple waves as applied specifically to non-dispersive, non-dissipative dust acoustic waves.

Using the Boltzmann relations for n_e and n_i, the dust density n_d is expressed in terms of the electrostatic potential, φ, as[40]

$$n_d = [n_{i0}\exp(-e\varphi/kT_i) - n_{e0}\exp(e\varphi/kT_e)]/Z_d. \quad (6)$$

The simple wave solutions for the dust fluid velocity and the potential obtained by Eliasson and Shukla[26] are

$$\frac{\partial \varphi}{\partial t} + \Lambda(\varphi)\frac{\partial \varphi}{\partial x} = 0, \quad \text{and} \quad \frac{\partial u_d}{\partial t} + \Lambda(\varphi)\frac{\partial u_d}{\partial x} = 0, \quad (7)$$

where

$$\Lambda(\varphi) = \frac{u_d}{C_{de}} + \sqrt{\frac{n_{i0}e^{-e\varphi/kT_i} - n_{e0}e^{e\varphi/kT_e}}{n_{i0}e^{-e\varphi/kT_i} + n_{e0}e^{e\varphi/kT_e}}}, \quad \text{with}$$

$$C_{de} = \sqrt{\frac{Z_d kT_e}{m_d}}.$$

The Eqs. (7) were solved numerically using the initial [t = 0 in Fig. 4(a)] dust acoustic waveform, to obtain u_d and φ, and the dust density. The dust density was then obtained using a Taylor expansion of Eq. (6) with respect to φ. The time evolution of the dust density is shown in Fig. 4(b). The numerical solutions predict a shock speed slightly less than but very close to the measured speed and also show that the wave steepens in a time $\sim$ 20 – 30 ms, in very good agreement with the observations. Since the theory contained no dissipation, only non-stationary solutions are obtained, so that the shock front steepened to the point thickness approached zero at which point the numerical solutions broke down. Overall, however, the simple wave solutions based on the theory of Eliasson and Shukla[26] provided an excellent representation of the observations, indicating that this simple nonlinear theory was sufficient to capture the essential physics of the observed dust acoustic shock waves.

VI. SUMMARY AND CONCLUSIONS

In this article, experimental observations of nonlinear dust acoustic waves and dust acoustic shock waves have been presented. Dust acoustic waves observed in typical discharge plasmas are spontaneously excited by the relative ion/dust drift instability. The waveforms of the travelling dust acoustic waves tend to have sharper wave crests and flatter wave troughs. We have interpreted this tendency in terms of a simple second-order wave theory in which a first harmonic wave is generated by the nonlinear physics and the addition of this harmonic content naturally leads to waveforms that describe the observed waveforms nicely. For experimental conditions under which highly nonlinear dust acoustic waves were produced, the waves exhibited self-steepening and evolved into shock waves. A theoretical formalism based on the Riemann solution of the fully nonlinear continuity and momentum equations for the dust fluid, with electrons and ions treated using the Boltzmann relations, was applied to the shock wave observations. Numerical solutions for the evolution of the initial dust acoustic pulses observed in the experiment were obtained, which were able to reproduce the basic features of self-steepening and shock formation.

Finally, we comment that the interpretation of the nonlinear dust acoustic wave phenomena was guided in part by consideration of complimentary phenomena occurring in the fields of acoustics (macrosonics) and ocean wave engineering, disciplines in which the study of nonlinear wave phenomena has been ongoing for over 100 years.

ACKNOWLEDGMENTS

This work was supported by DOE Grant No. DE-FG01-04ER54795 and NSF Grant No. PHY-0923141.

[1]For example, a solid spherical glass particle having a diameter of 1 μm, immersed in a plasma having electron and ion temperatures, T_e (= 100 T_i) = 2.5 eV, has a mass $\sim 10^{-15}$ kg, and a charge ~ -2000 e.
[2]The DA wave was first discussed by P. K. Shukla at the First Capri Workshop on Dusty Plasmas in May of 1989, which had an attendance of 17. The proceedings of the workshop can be found at http://www.physics.uiowa.edu/~rmerlino/CAPRIproceedings.pdf.
[3]N. N. Rao, P. K. Shukla, and M. Y. Yu, Planet. Space Sci. **38**, 543 (1990).
[4]N. D'Angelo, Planet. Space Sci. **38**, 1143 (1990).
[5]J. H. Chu, J.-B. Du, and I. Lin, J Phys. D: Appl. Phys. **27**, 296 (1994).
[6]N. D. Angelo, J Phys. D: Appl. Phys. **28**, 1009 (1995).
[7]A. Barkan, R. L. Merlino, and N. D'Angelo, Phys. Plasmas **2**, 3563 (1995).
[8]C. Thompson, A. Barkan, N. D'Angelo, and R. L. Merlino, Phys Plasmas **4**, 2331 (1997).
[9]T. Trottenberg, D. Block, and A. Piel, Phys. Plasmas **13**, 042105 (2006).
[10]E. Thomas, Jr., R. Fisher, and R. L. Merlino, Phys. Plasmas **14**, 123701 (2007).
[11]I. Pilch, T. Reichstein, and A. Piel, Phys. Plasmas **16**, 123709 (2009).
[12]J. D. Williams and J. Duff, Phys. Plasmas **17**, 033702 (2010).
[13]H. R. Prabhakara and V. L. Tanna, Phys. Plasmas **3**, 3176 (1996).
[14]V. E. Fortov, A. G. Khrapak, S. A. Khrapak, V. I. Molotkov, A. P. Nefedov, O. F. Petrov, and V. M. Torchinsky, Phys. Plasmas **7**, 1374 (2000).
[15]E. Thomas Jr. and R. L. Merlino, IEEE Trans. Plasma Sci. **29**, 152 (2001).
[16]M. Schwabe, M. Rubin-Zuzic, S. Zhdanov, H. M. Thomas, and G. E. Morfill, Phys. Rev. Lett. **99**, 095002 (2007).
[17]L.-W. Teng, M.-C. Chang, Y.-P. Tseng, and I. Lin, Phys. Rev. Lett. **103**, 245005 (2009).
[18]R. L. Merlino, Phys. Plasmas **16**, 124501 (2009).
[19]M. Rosenberg, Planet. Space Sci., **41**, 229 (1003); J. Vac. Sci. Technol. A **14**, 631 (1996); J. Plasma Phys. **67**, 235 (2002).
[20]T. M. Flannigan and J. Goree, Phys. Plasmas **17**, 123702 (2010).
[21]T. M. Flannigan and J. Goree, Phys. Plasmas **18**, 013705 (2011).

[22]J. R. Heinrich, S.-H. Kim, J. K. Meyer, and R. L. Merlino, Phys. Plasmas **18**, 113706 (2011).
[23]A new perspective on the mechanism for driving dust acoustic waves has been discussed by A. Piel, AIP Conf. Proc. **1397**, 50 (11).
[24]A photograph of (non-sinusoidal) Stokes waves generated in a large water basin by a wavemaker is shown in plate 195 of M. Van Dyke's, *An Album of Fluid Motion* (The Parabolic, Stanford, CA, 1982). A historical discussion of Stokes' 19th century work on water wave theory appears in A. D. D. Craik, Annu. Rev. Fluid. Mech. **37**, 23 (2005). Practical applications of water wave theory are discussed in R. G. Dean and R. A. Dalrymple, Water Wave Mechanics for Engineer and Scientists (Applied Publishers Limited, New Dehli, 2001). In fluid dynamics, first order (linearized) wave theory is referred to as "Airy theory" and higher order wave theories as "Stokes theory.
[25]J. R. Heinrich, S.-H. Kim, and R. L. Merlino, Phys. Rev. Lett. **103**, 115002 (2009).
[26]B. Eliasson and P. K. Shukla, Phys. Rev. E **69**, 067401 (2004).
[27]T. An, R. L. Merlino, and N. D'Angelo, J. Phys. D: Appl. Phys. **27**, 1906, (1994).
[28]All probe measurements were made in dust-free plasmas because it is well-known that electric probes disturb the dust; see, e.g., E. Thomas Jr., R. L. Merlino, and K. Avinash, Phys. Plasmas **11**, 1770 (2004).
[29]P. K. Shukla and A. A. Mamun, *Introduction to Dusty Plasma Physics* (IOP, Bristol, 2002), p. 36.
[30]Photron FASTCAM 1024, which has a linear response to light intensity and image sizes of 1024 by 1024 pixels.
[31]In acoustics, sound waves are usually designated by the "excess pressure," or the difference between the pressure in the presence of the wave and the undisturbed gas pressure.
[32]Details of the derivation of the second-order dust acoustic wave theory are given in, R. L. Merlino, Phys. Scr. **85**, 035506 (2012).
[33]P. M. Morse and K. Uno Ingard, *Theoretical Acoustics* (McGraw-Hill, New York, 1968), p. 866.
[34]One effect that emerges from the second-order theory of sound waves is radiation pressure. The time average of first order term for the excess pressure vanishes, whereas the time average of the second-order term does not, and this is in effect a static excess pressure or momentum flux. This is generally referred to as the Rayleigh pressure and is discussed in R. B. Lindsay's *Mechanical Radiation* (McGraw Hill, New York, 1930), p. 292. The corresponding effect for nonlinear water waves is known as the Stokes' drift which is discussed by Craik in his article cited in Ref. 24. We have observed a similar phenomenon of a dust drift in a large-amplitude dust acoustic wave. This will be reported in a separate publication.
[35]The Fourier series for a sawtooth wave of the form $f(x) = x$, $0 < x < 1$, involves the sum of terms of the form: $\sin(n\pi x)/nn$.
[36]A. A. Mamun and R. A. Cairns, Phys. Rev. E **79**, 055401 (2009).
[37]M. R. Gupta, S. Sarkar, S. Ghosh, M. Debnath, and M. Khan, Phys. Rev. E **63**, 046406 (2001).
[38]H. Asgari, S. V. Muniandy, and C. S. Wong, Phys. Plasmas **18**, 013702 (2011).
[39]See, for example, L. D. Landau and E. M. Lifshitz, *Fluid Mechanics* (Addison Wesley, Reading, MA, 1959), p. 366, for a discussion of the Riemann solution as applied to sound waves, and D. Montgomery, Phys. Rev. Lett. **19**, 1465 (1967), for an application to nonlinear ion acoustic waves.
[40]Note that the shock wave equations presented here are fully dimensional, while those in Ref. 26 use normalized variables.